Pre-salt time-lapse seismic monitoring with joint 4D FWI

Filipe Rudrigues, Gabriel Brando, Danilo Albuquerque, Danilo Froes, Benjamin Huard, Luis Cypriano, Roberto Pereira, and Adel Khalil, Viridien*

Summary

Historically, Brazilian pre-salt fields have been imaged by narrow-azimuth towed-streamer (NATS) data. More recently, ocean bottom node (OBN) acquisitions have been employed to image and monitor already producing fields. In cases as such, 4D seismic monitoring is only possible via NATS/OBN hybrid pairs, where NATS and OBN data sets serve as "base" and "monitor", respectively. This hybrid configuration implies low repeatability. Extracting subtle 4D changes in hard pre-salt carbonate reservoirs can be challenging. Considering this, we propose a joint 4D full-waveform inversion (FWI) formulation to overcome low repeatability between different seismic surveys. We demonstrate promising results using a field data set from Santos Basin, where realistic 4D anomalies can be identified.

Introduction

Time-lapse seismic monitoring is an important tool for optimizing oil recovery. The method is based on understanding subsurface changes throughout a period of production activities. Cypriano et al. (2019) and Cruz et al. (2021) reported the results of the first 4D seismic imaging for Brazilian pre-salt reservoirs. They showed that realistic 4D information, with amplitudes of around 2%, can be retrieved when comparing data from two OBN acquisitions, spanning a production period of approximately 2 years.

Time-lapse monitoring is crucial for development of pre-salt fields; however, seismic data availability and quality is unevenly distributed over time. In early exploration stages, NATS data is largely available throughout the pre-salt polygon. On the other hand, OBN data, with full-azimuthal coverage and longer offset ranges, only started to be acquired less than a decade ago. Several fields may have NATS data acquired before production and OBN data acquired only after a few years of production. Deriving 4D information between NATS and OBN data sets is a possible solution, but subject to considerable unrepeatability in acquisition geometry. In carbonate pre-salt fields, where subtle 4D differences are expected, overcoming the 4D signal-to-noise barrier can be challenging.

There have been previous attempts to extract 4D signal between different types of surveys. Wang et al. (2017) show the importance of least-squares migration (LSM), as well as dedicated 4D processing, to attenuate high-amplitude background noise that arise from poor repeatability between NATS and OBN geometries in the Gulf of Mexico. The context of the Brazilian pre-salt, with deep reservoirs below thick and stratified evaporitic deposits, presents its own challenges. To illustrate this, Figure 1 shows an inline from a pre-salt field. The baseline is a NATS data set acquired in 2012, while the monitor is an OBN data set acquired in 2021. The RTM baseline image is shown in Figure 1a. Figure 1b shows the 4D difference after a dedicated 4D pre-processing sequence including matching, binning, and deghosting. Due to acquisition discrepancies, the obtained 4D difference shows unrealistic strong amplitudes. By using an image-domain single-iteration LS-RTM approach (Wang et al., 2016), we observe a reduction in 4D noise (Figure 1c). This can be attributed to LSM's ability to compensate some of the acquisition and illumination effects. The image also shows a potential 4D anomaly below the base of salt and near a well (green line). However, the background noise is still above 10% at the reservoir depth. Such noise level may lead to erroneous or incomplete 4D interpretation, as the expected 4D changes are in the order of 2%.

High-frequency FWI and its byproduct, FWI Imaging, can also be used for 4D monitoring (Li et al., 2021). It honors the physics of the earth better than RTM or LS-RTM. It also benefits from full-wavefield modeling and has proven to be effective when combined with tailored cost functions, such as in Time-Lag FWI (TLFWI, Zhang et al., 2018).

There are several strategies in the literature for tackling the challenges of time-lapse 4D FWI (Plessix et al., 2010; Routh et al., 2012; Zheng et al., 2011; Hicks et al., 2016; Zhou and Lumley, 2021; Fu and Innanen, 2023). For example, Figure 1d shows the velocity 4D difference obtained with the parallel strategy (Plessix et al., 2010), in which both vintages are inverted independently starting from the same initial model. It indicates a reservoir anomaly around the well, as observed in the RTM and LS-RTM results. However, some unexpected remaining 4D noise at the top of salt and in the pre-salt can still be observed. Despite being better suited for the level of physics complexity, FWI still deals with an unstable, ill-posed inverse problem, prone to severe ambiguity. To overcome this, we developed a new joint 4D FWI formulation. It is designed to reduce the dependence of the results on the acquisition geometry of the data.

Joint 4D FWI

To attenuate non-repeatability between different seismic surveys, we developed a novel joint 4D FWI scheme. In this approach, both vintages are inverted starting from the same initial model. However, at each iteration, the updates for baseline and monitor models are constrained with geometrical information from the other survey, which enter

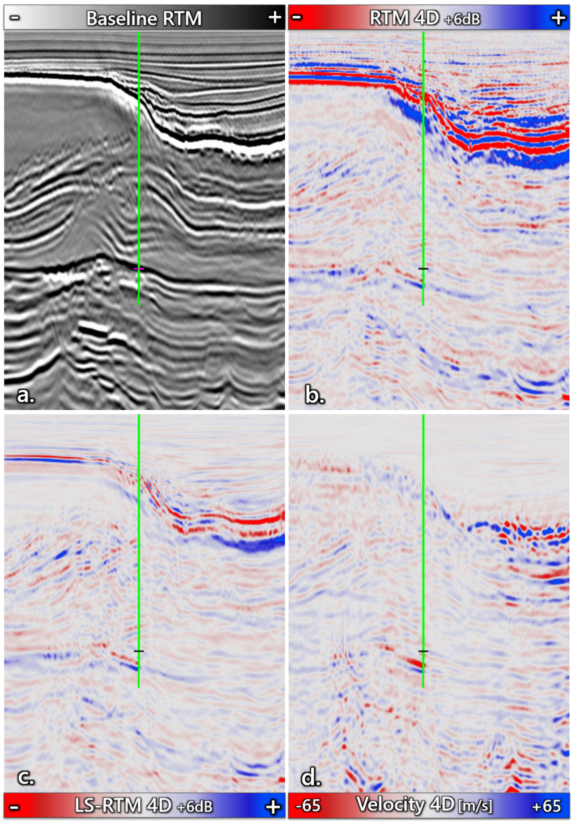

Figure 1: (a) RTM image of the NATS monitor data. (b) 4D RTM image difference. (c) 4D LS-RTM image difference. (d) 4D velocity difference based on FWI parallel strategy. Well is shown as green line. A 90° rotation was applied to the RTM and LS-RTM 4D image differences to allow for the comparison with the FWI 4D velocity difference.

as a preconditioning to each gradient. This geometrical information can be extracted from the Hessian (Pratt et al., 1998) and are estimated on top of Hessian products (see Métivier et al., 2014). We start with a general 4D cost function of the form

$$C[m_B, m_M] = C_B[m_B] + C_M[m_M], \quad (1)$$

where m_B and m_M are the baseline and monitor models, and C_B and C_M are the cost functions for each vintage. For our application, C_B and C_M are the time-lag cost functions (Zhang et al., 2018). The update for each FWI iteration can be written as the preconditioned gradients of the 4D cost function (1):

$$\Delta m_B = -P_B g_B, \qquad \Delta m_M = -P_M g_M, \quad (2)$$

where the preconditioners P_B and P_M represent approximate inverses of the respective Hessian operators, and g_B and g_M

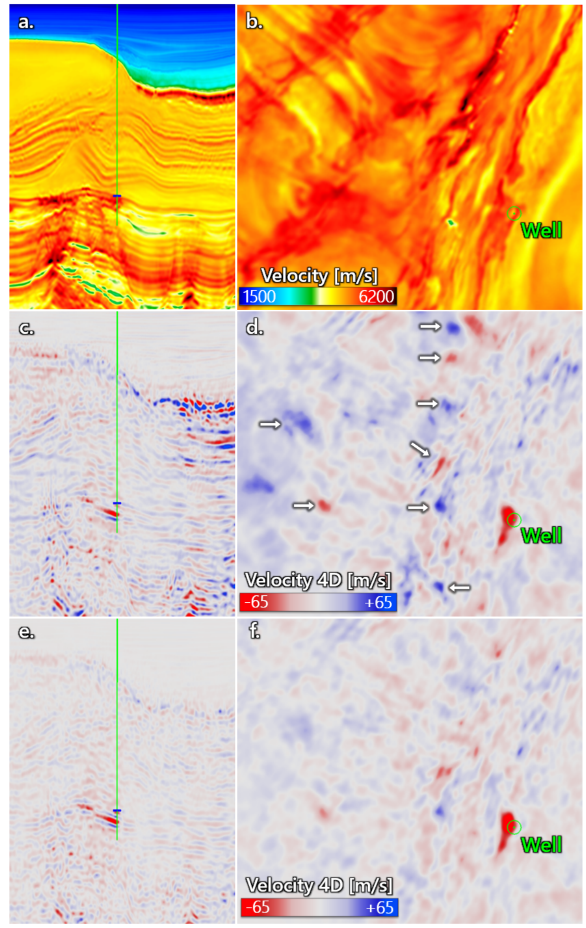

Figure 2: (a) Line view and (b) reservoir depth slice of the input velocity model. (c) Line view and (d) reservoir depth slice of the 4D velocity difference obtained with the parallel strategy 4D FWI approach. (e) Line view and (f) reservoir depth slice of the 4D velocity difference obtained with the joint 4D FWI approach. One well trajectory is shown as a green line.

represent the gradients over m_B and m_M, respectively. Since the preconditioners are not true inversions of the Hessian, they do not fully compensate for the wave propagation effects in the gradient. Furthermore, there are still imprints of the acquisition geometries in each update.

To attenuate this effect, we seek a new set of preconditioners P_B^γ and P_M^γ that approximately invert for the Hessians on a given search space direction γ representative of the current FWI iteration in a manner that is consistent between both surveys. We obtain them through a minimization process in terms of the original preconditioners, with the constraint

$$P_B^\gamma H_B \gamma = P_M^\gamma H_M \gamma, \quad (3)$$

10.1190/image2024-4099984.1

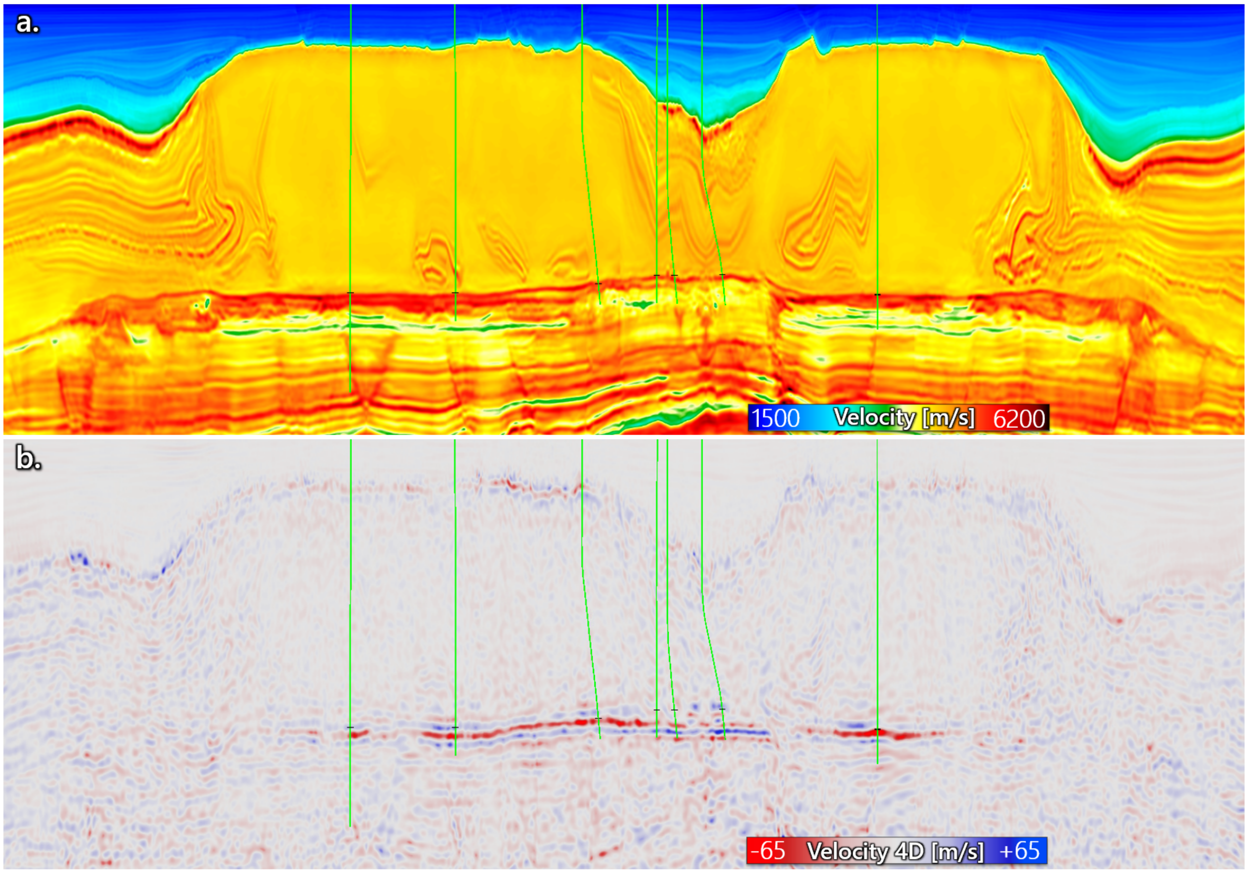

Figure 3: Arbitrary line passing through wells of the study area for (a) the input velocity model and (b) the 4D velocity difference obtained with the joint 4D FWI approach. Well trajectories are show as green lines.

which imposes the geometrical effects of the monitor acquisition into the baseline preconditioner, and vice-versa. In particular, the null-space of the monitor Hessian is inherited by the baseline preconditioner, and vice-versa.

Pre-salt field case study

To obtain our results, we used TLFWI separately for each vintage, with the input data sets having been through 4D pre-processing to ensure consistency. The OBN data set was limited to the NATS acquisition azimuth to reduce non-repeatability. As a reference for interpreting the 4D difference results, Figures 2a and 2b show a line view and a reservoir depth slice of the input velocity model, respectively. This velocity model was obtained with a full-azimuth OBN inversion up to 30 Hz. Figures 2c and 2d show the velocity 4D difference obtained with the parallel strategy. White arrows indicate reservoir regions of unrealistic anomalies, with no relation to wells. Figures 2e and 2f show the 4D difference obtained with the proposed joint 4D FWI. By comparing the results, we observed that the joint 4D FWI shows a general attenuation of 4D noise, both inside and outside the target reservoir region, while keeping the expected 4D signal near the well unchanged.

Figures 3a and 3b show an arbitrary line of the input velocity model and the 4D velocity difference obtained with the joint 4D FWI approach, respectively. The selected line passes through different wells in a region of thick evaporitic deposits. Anomalous amplitudes can be identified in Figure 3b, at shallow pre-salt depths. The 4D anomalies are found within the cluster of wells and their depths seem in agreement with other pre-salt fields, as observed in a previous case study (Cypriano et al., 2019). This gives some confidence in the obtained results.

The performance of our joint 4D FWI approach can also be evaluated by comparing its results with those obtained with the LS-RTM method. To do this comparison in the image domain, we derived the FWI Images from the base and monitor FWI velocity models and computed the difference between them. The FWI Images were obtained by

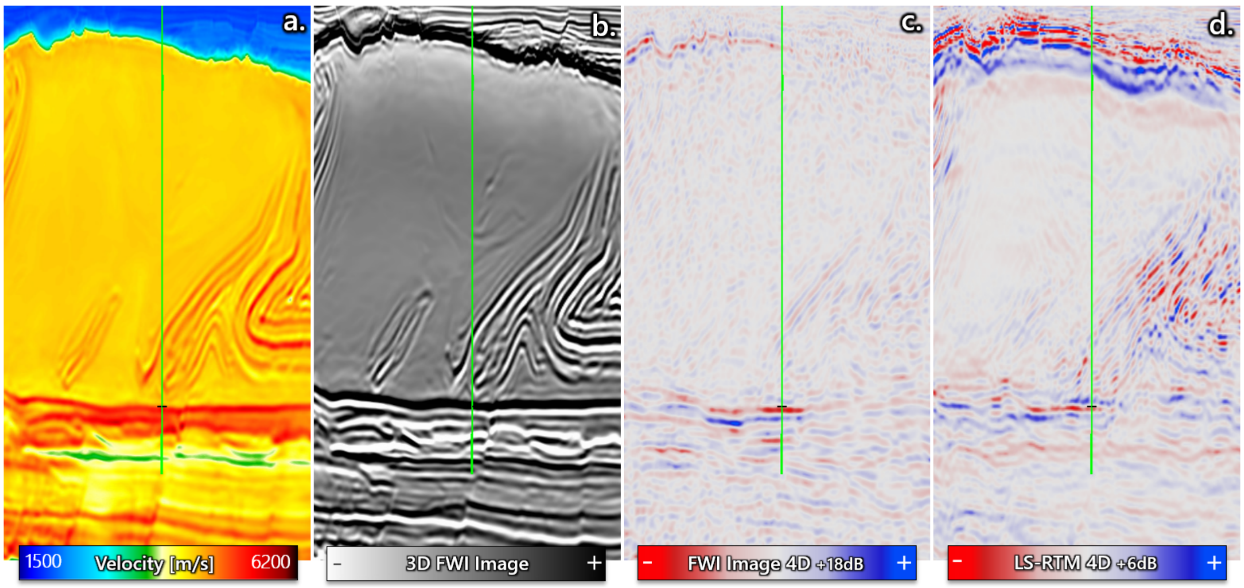

Figure 4: Line view for (a) the baseline velocity model, (b) the baseline 3D FWI Image, (c) the FWI Image 4D difference, and (b) the LS-RTM 4D difference. Well trajectory is shown as green line.

computing the derivatives of the velocity fields along the normal direction of reflectors, assuming the velocity-to-impedance relationship described in Zhang et al. (2020). Due to the use of full-wavefield modeling, FWI Imaging is known to benefit from improved pre-salt illumination when compared to other imaging methods (Dolymnyj et al., 2022; Azevedo et al., 2023; Brando et al., 2023; Henrique et al.; 2023).

Figures 4a and 4b show a line view of the baseline velocity model and the corresponding baseline 3D FWI Image, respectively. The related FWI Image 4D difference for the same line view can be seen in Figure 4c. For comparison purposes, Figure 4d shows the LS-RTM 4D difference. A well trajectory is shown as a green line in all displays. A potential 4D anomaly at pre-salt depths can be seen around the well trajectory in both the FWI Image and LS-RTM 4D difference displays. The anomaly found in the FWI Image result is more pronounced in relation to the background 4D noise when compared to the LS-RTM results. The FWI Image 4D difference shows less significant noise at the top of salt and within the intra-salt layers. These are regions where no real 4D information is expected. This means that, in this specific application, the proposed joint 4D FWI is yielding more realistic 4D information than the conventional LS-RTM method.

The difference between LS-RTM and FWI could be attributed to multiple factors. FWI utilizes direct wave-equation modeling in contrast to the linearized Born modeling of LS-RTM. Furthermore, FWI is iterative in nature and utilizes a different cost function. These factors together help to produce a subsurface model that yields a better match with real data. This leads to reduction of non-geological 4D noise related to geometrical unrepeatability.

Results indicate that the interpretation of 4D information can benefit from the presented joint 4D FWI. Interpretation of the obtained 4D information and their validation is out of the scope of this work and requires domain experts.

Conclusions

This work proposed a new joint 4D FWI formulation, motivated by the need for performing time-lapse seismic monitoring when baseline and monitor data sets were acquired with different acquisition geometries. Results showed its potential when applied to a pair of NATS-OBN data sets acquired over a pre-salt area. The new approach is particularly well suited for seismic monitoring within the context of Brazilian pre-salt fields. The full-wavefield modeling of FWI is appropriate for the level of imaging complexity related to the deep pre-salt targets, and most of the pre-salt fields have only NATS data available before production, with OBN data being acquired more recently.

Acknowledgments

We thank Petrobras and partners for the permission to publish this work.

REFERENCES

Azevedo, J., G. Pacheco, K. Pereira, and L. Cypriano, 2023, Revealing pre-salt structures underneath volcanics with FWI imaging: 18th International Congress of the Brazilian Geophysical Society, SBGf, Expanded Abstracts.

Brando, G., B. Huard, and L. Cypriano, 2023, Imaging the presalt with elastic FWI using OBN data: Third International Meeting for Applied Geoscience & Energy, SEG/AAPG, Expanded Abstracts, 685–689, doi: https://doi.org/10.1190/image2023-3917169.1.

Cruz, N. M., J. M. Cruz, L. M. Teixeira, M. M. da Costa, L. B. de Oliveira, E. N. Urasaki, T. P. Bispo, M. de Sá Jardim, M. H. Grochau, and A. Maul, 2021, Tupi Nodes pilot: A successful 4D seismic case for Brazilian presalt reservoirs: The Leading Edge, **40**, 886–896, doi: https://doi.org/10.1190/tle40120886.1.

Cypriano, L., Z. Yu, D. Ferreira, B. Huard, R. Pereira, F. Jouno, A. Khalil, E. Urasaki, N. Cruz, A. Yin, D. Clarke, and C. Jesus, 2019, OBN for pre-salt imaging and reservoir monitoring — potential and road ahead: 16th International Congress of the Brazilian Geophysical Society, SBGf, Expanded Abstracts.

Dolymnyj, C., F. Rudrigues, A. Porto, L. Galves, and A. Ovalles, 2022, Assessing FWI imaging's potential to tackle illumination issues and internal multiples in the Brazilian presalt: Second International Meeting for Applied Geoscience & Energy, SEG/AAPG, Expanded Abstracts, 782–786, doi: https://doi.org/10.1190/image2022-3749870.1.

Fu, X., and K. A. Innanen, 2023, Stepsize sharing in time-lapse full-waveform inversion: Geophysics, **88**, no. 2, M59–M70, doi: https://doi.org/10.1190/geo2022-0094.1.

Henrique, A., L. Felão, S. Barragan, and F. Jouno, 2023, Elastic FWI imaging of a complex presalt structure using NATS data: Third International Meeting for Applied Geoscience & Energy, SEG/AAPG, Expanded Abstracts, 605–609, doi: https://doi.org/10.1190/image2023-3913327.1.

Hicks, E., H. Hoeber, M. Houbiers, S. P. Lescoffit, A. Ratcliffe, and V. Vinje, 2016, Time-lapse full-waveform inversion as a reservoir-monitoring tool — A North Sea case study: The Leading Edge, **35**, 850–858, doi: https://doi.org/10.1190/tle35100850.1.

Li, N., Z. Yu, R. To, M. Wang, Y. Xie, and D. Dickinson, 2021, 4D FWI using towed-streamer data: A case study near Laverda oil field: First International Meeting for Applied Geoscience & Energy, SEG, Expanded Abstracts, 622–626, doi: https://doi.org/10.1190/segam2021-3582747.1.

Métivier, L., F. Bretaudeau, R. Brossier, S. Operto, and J. Virieux, 2014, Full waveform inversion and the truncated Newton method: Quantitative imaging of complex subsurface structures: Geophysical Prospecting, **62**, 1353–1375, doi: https://doi.org/10.1137/16M1093239.

Plessix, R.-E., S. Michelet, H. Rynja, H. Kuehl, C. Perkins, J. W. de Maag, and P. Hatchell, 2010, Some 3D applications of full waveform inversion: 72nd Conference and Exhibition, EAGE, Workshops and Fieldtrips.

Pratt, G., C. Shin, and G. J. Hick, 1998, Gauss–Newton and full Newton methods in frequency–space seismic waveform inversion: Geophysical Journal International, **133**, 341–362, doi: https://doi.org/10.1046/j.1365-246X.1998.00498.x.

Routh, P., G. Palacharla, I. Chikichev, and S. Lazaratos, 2012, Full wavefield inversion of time-lapse data for improved imaging and reservoir characterization: 82nd Annual International Meeting, SEG, Expanded Abstracts, 1–6, doi: https://doi.org/10.1190/segam2012-1043.1.

Wang, P., A. Gomes, Z. Zhang, and M. Wang, 2016, Least-squares RTM: Reality and possibilities for subsalt imaging: 86th Annual International Meeting, SEG, Expanded Abstracts, 4204–4209, doi: https://doi.org/10.1190/segam2016-13867926.1.

Wang, Z., R. Huang, Y. Xuan, Q. Xu, S. Morton, and B. Kuntz, 2017, Improving OBS-streamer 4D imaging by least-squares migration: 87th Annual International Meeting, SEG, Expanded Abstracts, 5819–5823, doi: https://doi.org/10.1190/segam2017-17739944.1.

Zhang, Z., J. Mei, F. Lin, R. Huang, and P. Wang, 2018, Correcting for salt misinterpretation with full-waveform inversion: 88th Annual International Meeting, SEG, Expanded Abstracts, 1143–1147, doi: https://doi.org/10.1190/segam2018-2997711.1.

Zhang, Z., Z. Wu, Z. Wei, J. Mei, R. Huang, and P. Wang, 2020, FWI Imaging: Full-wavefield imaging through full-waveform inversion: 90th Annual International Meeting, SEG, Expanded Abstracts, 656–660, doi: https://doi.org/10.1190/segam2020-3427858.1.

Zheng, Y., P. Barton, and S. Singh, 2011, Strategies for elastic full waveform inversion of time-lapse ocean bottom cable (OBC) seismic data: 81st Annual International Meeting, SEG, Expanded Abstracts, 4195–4200, doi: https://doi.org/10.1190/1.3628083.

Zhou, W., and D. Lumley, 2021, Central-difference time-lapse 4D seismic full-waveform inversion: Geophysics, **86**, no. 2, R161–R172, doi: https://doi.org/10.1190/segam2019-3213915.1.